Research Article Vol. 30, No. 4 / 14 Feb 2022 / Optics Express 6003
Optics EXPRESS

Flexible composite film with artificial opal photonic crystals for efficient all-day passive radiative cooling

FENG NAN,[1] YU-FU ZHU,[1] HUAI-XIN WEI,[2] YI LIN,[1,3] BAOLU FAN,[1] AND LEI ZHOU[1,4]

[1] *Faculty of Mathematics and Physics, Huaiyin Institute of Technology, Huai'an 223003, China*
[2] *Jiangsu Key Laboratory for Environment Functional Materials School of Chemical Biology and Materials Engineering, Suzhou University of Science and Technology, Suzhou 215009, China*
[3] *linyihit@hyit.edu.cn*
[4] *leizhou@hyit.edu.cn*

Abstract: All-day passive radiative cooling has recently attracted broader attention for its potential as a viable energy technology. Although tremendous progress has been achieved, the design and fabrication of low-cost high-efficiency radiators for all-day passive radiative cooling remains a challenge. Herein, we report a new type of flexible composite radiator film with built-in artificial opal-like structures for all-day passive radiative cooling. Using artificial opal structure concepts, the proposed polydimethylsiloxane (PDMS) radiator film with embedded polystyrene (PS) microsphere photonic crystals exhibits a sufficiently high solar reflectance of ~92.7% when in a direct sunlight region, and a thermal emittance of ~93.6% within the atmospheric window. Without the need for traditional reflectors like silver or aluminum foils, this composite film realizes subambient temperature reduction of ~4.8 °C in direct sunlight and ~8.5 °C during the night. This work provides a new fabrication approach for the low-cost production of structural polymer films for high performance and potential real word applications.

1. Introduction

Traditional human refrigeration activities, accounting for 20% of the world's electricity, consume tremendous amount of energy and thus aggravate undesirable the greenhouse effect [1–3]. Passive radiative cooling, generating a cooling effect by dissipating an object's heat into outer ultracold (3 K) space through an atmospheric transparency window (8-13 μm) without consumption of any external energy input, has gains much attention as an emerging and renewable heat manipulation means [4,5]. While nighttime radiative cooling has been extensively investigated and proved [6,7], the peak demand for cooling shifts to the daytime. To achieve efficient daytime radiative, a radiator structure should be designed to synchronously realizing both high solar light reflectance and strong thermal emitter in the atmospheric transparency window. Therefore, tremendous effort has been devoted to the design and construction of the passive daytime radiators. For example, polymers or polymer-dielectric composites on metallic reflectors (*e.g.*, silver or aluminum) [8,9], polymer-dielectric composites [10], and inorganic pigments-polymeric composites [11,12]. Recently, artificial photonic structured radiators, such as metal-dielectric photonic structure [4], multilayer stacks [13], nanoporous polymer matrix composite [14], bio-inspired three-dimensional pores [15], microvoids [16], and symmetrically shaped conical metamaterial [17], have been theoretically and experimentally investigated to achieve desired effect of daytime radiative cooling. However, most of advanced thermal photonic radiators suffer from complicated manufacture procedures and problems with fabrication costs [18–20]. Although the reported approach provided a relative simple fabrication procedure, sacrificial template process involved in high-temperature heating is still required. Moreover, it is found that some inorganic pigments (*e.g.*,

#448714 https://doi.org/10.1364/OE.448714
Journal © 2022 Received 15 Nov 2021; revised 29 Jan 2022; accepted 29 Jan 2022; published 9 Feb 2022

Optics EXPRESS

zinc oxide and titanium dioxide) are reported to be harmful to human body [15,21]. Therefore, it is expected that the radiators associated with inorganic pigments would gradually withdraw from the cooling strategies.

Additionally, it is well known that opal structures, which referred as close-packed face-centered cubic (FCC) crystals with 74 vol% periodically arranged SiO_2 nanospheres, can achieve iridescent colors in the visible spectrum resulting from Bragg diffraction [22,23]. Inspired by the natural opal structures, herein we built a new type of flexible composite film with artificial opal photonic crystals for both efficient daytime and nighttime radiative cooling via a facile self-assembling method. The proposed PDMS radiator film with embedded polystyrene (PS) microsphere photonic crystals is able to strongly repel the impinging sunlight while enhancing thermal radiation in the atmospheric window simultaneously. Furthermore, unlike high specular reflection capability of the traditional radiator combined with metallic mirrors, the free-standing composite polymer radiator composed of organic materials not only avoids detrimental visual effects and ultraviolet absorption [8,24], but also is harmless to human body [15]. By optimizing and engineering the PS microspheres size, the acquired structural polymer radiator film achieves a high total reflectivity of ~92.7% in the major sunlight region and a favorable emissivity of ~93.6% within the atmospheric window, respectively. Due to such desirable solar irradiation reflection and infrared thermal radiation, the structured polymer radiator yields subambient temperature reduction of ~4.8 °C under direct sunshine. By taking advantage of the light steering capability of the artificial opal photonic crystals composed of PS microspheres and cooperatively selective emission behavior of PDMS material, the developed composite polymer film is of great potential for advancing radiative cooling as a viable energy technology.

2. Results and discussion

2.1. Device fabrication

Figure 1(a) schematically illustrates the fabrication procedure of the composite film with built-in photonic crystals structure. Firstly, the artificial opal structure composed of the hexagonal close-packed polystyrene (PS) microsphere arrays are fabricated on the pre-cleaned silicon substrate using a simply and widely employed self-assembling method [25,26]. Subsequently, the precursors of PDMS solution are spin-coated onto the surface of the opal structure and accordingly infiltrated into their voids in a vacuum oven due to its very low-surface-energy (19.6 dyn cm^{-1}) [27]. After annealing procedure for solidifying PDMS precursors, the free-standing composite polymer radiator film is successfully acquired by peeling off from the substrate (See details in Experimental section). To characterize the morphology of the PS microspheres array and the composite film, the scanning electron microscopy (SEM) images of the PS microsphere templates and the composite film are performed and presented in Fig.1b-e, respectively. It can be seen that the two elaborately selected diameters ($D = 1$ and 4 μm) of PS microspheres are assembled as multi-layer FCC crystals (See details in Theoretical analysis) with ~70 vol% (Fig. 1(b) and (c)), showing a typical artificial opal structure [28–22]. Meanwhile, the surface of the composite film displays relatively smooth topography, signifying the opal structure has been successfully stripped from the Si substrate and is deliberately embedded into the PDMS film to form composite membrane (Fig. 1(d)).

2.2. Optical and outdoor thermal characterization

The total reflectance spectra of the PDMS films without and with artificial opal photonic crystals in the solar region are investigated. As depicted in Figure 2(a), compared with the negligible total reflectance of the planar PDMS film (~3%), the composite films with PS microspheres diameters of 1 μm and 4 μm yield much higher total reflectance of ~92.7% and ~90.1% in the solar irradiation range, respectively. This desirable reflectivity capability can be ascribed to

Optics EXPRESS

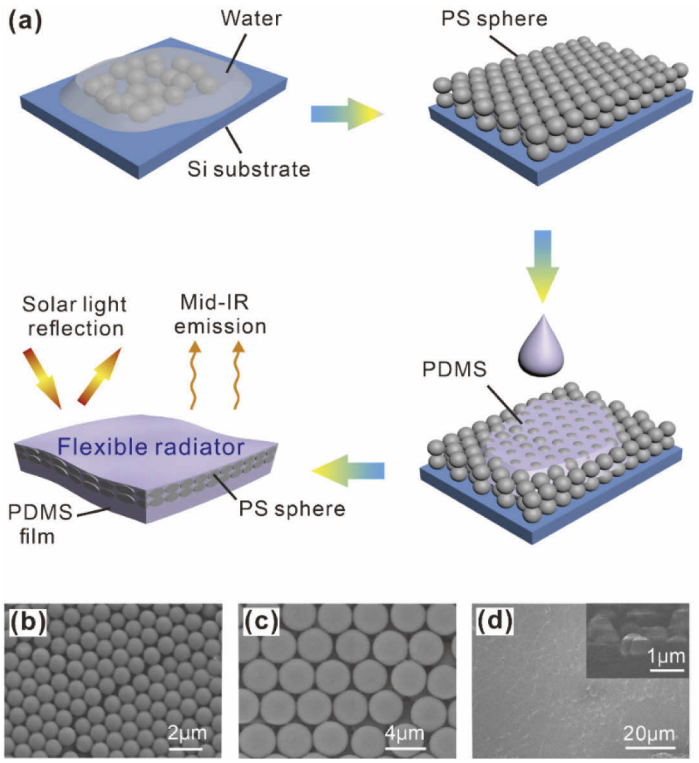

Fig. 1. Fabrication and characterization of the composite film. (a) Schematic illustration of the fabrication procedure of composite film with artificial opal photonic crystals structure. SEM images of the PS spheres template with diameter of b) 1 μm and c) 4 μm, respectively. (d) SEM image of the surface morphology of the composite film (D =1 μm). Inset depicts the zoom-in cross-section SEM image of the composite film. The thickness of PS spheres layer is about 4 times of its diameter.

the specially tailored opal photonic crystal structure, which keeps the solar heat accumulation on the structural film surface to a minimum. It is worth mentioning that the reflectivity of the both structured films gradually decrease as the increment of the wavelength within the near-infrared spectrum (1.5~2.5 μm). However, the solar irradiation during this specific region merely contributes a minor part of total solar irradiation and it has little impact on the average reflectance in the entire solar spectrum (0.3~2.5 μm). Compared with high transparent of the flat film (Fig. 2(b)), the as-obtained structural films (3.2 cm × 3.2 cm) with two different microsphere arrays (D = 1 and 4 μm, respectively) vividly display rather whitish appearance with high opacity (Fig. 2(c) and (d)), confirming the visible light scattering effect of the artificial opal photonic crystal structures. Specifically, this diffused reflectance effect avoids undesirable specular reflection, which always leads to detrimental visual effects on human and causes notorious threat to aircraft operations [30,31], and is thereby beneficial to practical application.

The large power density mismatch between the solar irradiation and the infrared thermal emissivity clearly requires a diurnal radiator to possess high absorptivity within the atmospheric transparency window. Meanwhile, by Kirchhoff's law, the absorptivity of a radiator corresponds to its emissivity [32]. Thereby, to quantitatively characterize the emissivity properties of the films, the absorptivity/emissivity spectra of the radiation films are furtherly measured and provided in Fig. 2(e). Compared with the reference flat film (~87.6%), the average emissivity values of the structured films with microsphere diameters of 1 μm and 4 μm can increase 6.6% (~93.6%) and

Optics EXPRESS

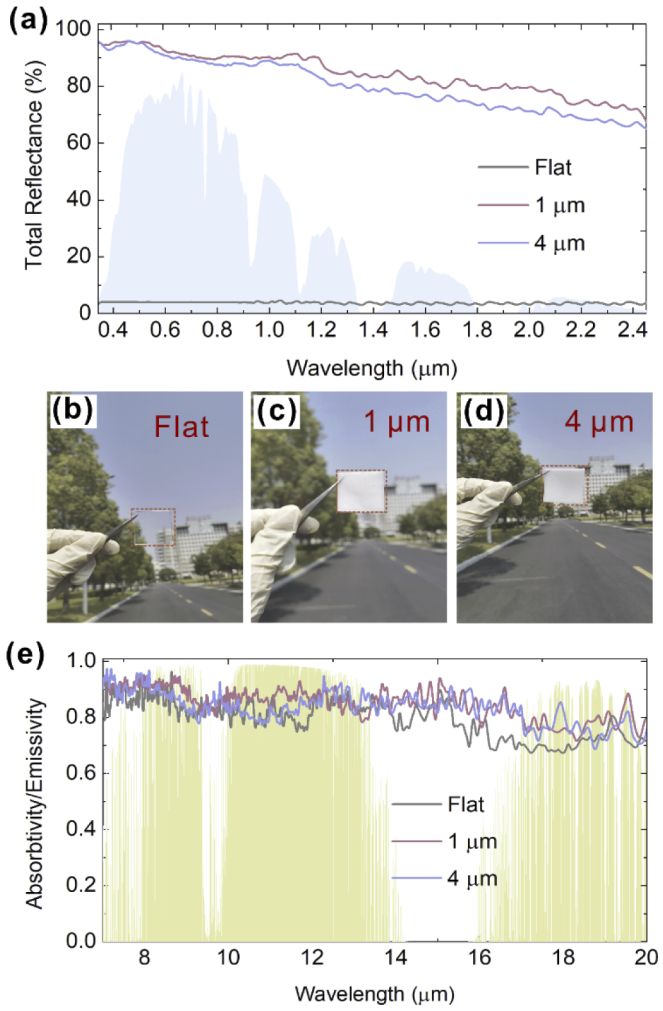

Fig. 2. (a) Measured reflectance spectra of the films without and with photonic crystals structure. (b-d) Photographs of the prepared films under direct sunlight. (e) Measured absorptivity/emissivity spectra of the radiation films.

5.13% (~92.1%) in the atmospheric transparency window. This feature directly illustrates that the introduction of the artificial opal crystal structure not only remarkably rejects the incident solar light, but also efficiently assist light absorption within the atmospheric transparency window. It should be emphasized that although the planar film exhibit attractive absorptivity in the mid-infrared (MIR) range due to the innate selective absorption property of PDMS material [33], which cannot be directly employed for diurnal radiative cooling because of its extremely weak reflectivity behavior for solar irradiation [20].

To practically investigate the cooling performance of the prepared samples, we conducted outdoor experiments on clear summer days at Huai'an, China (33.61° N, 119.02° W), by exposing the self-made experimental setups to the sky. As depicted in Figure 3(a), the prepared films are placed inside the self-made box constructing on the 1.5 m high concrete pedestal to minimize the parasitic heat gains from the extremely heated ground. Meanwhile, to suppress the nonradiative convective/conductive heat exchange with the ambient and simultaneously allow the sunlight directly irradiate the samples, the side and bottom walls comprising of 2.5 cm-thick polyurethane

Optics EXPRESS

plank with coefficient of heat conductivity of 0.02 $W \cdot m^{-1} \cdot K^{-1}$ are wrapped by aluminum foil and the transparent low-density polyethylene (LDPE) foils are employed as the transparent window. The result of the consistent 24 h outdoor temperature tests are displayed in Fig. 3(b). It can be observed that the structured films with microsphere diameters of 1 µm and 4 µm display a temperature of ~32.4 °C and ~33.1 °C under direct sunlight irradiation around 1:00 p.m (local time, 11:00-13:30, relative humidity = 54%, average solar irradiance = 860 W/m^2, and air temperature = 38 °C), respectively, much lower than that of the ambient temperature (~36.4 °C). Moreover, the two photonic crystal structured films also yield satisfied subambient cooling of ~8.5 °C and ~ 7.4 °C at night (24:00 - 4:00), respectively. These test results confirm that the proposed film structure is suitable for highly efficient all-day passive radiative cooling. Furthermore, the Yong's modulus values of both micro-spheres structured radiator films are measured as ~2.57 MPa, which is comparable to that of the bare PDMS film (~2.44 MPa), implying that the composited films still achieve a desirable flexible ability. This result demonstrated that our composited film is compatible with curved surfaces of objects. As displayed in Fig. 4(a) and (b), after being contacted for 15 min, the infrared digital photos are immediately recorded when the radiator films are removed from the rear cover of a cellphone. The bare rear cover of a cellphone's temperature is ~36.3 °C, while the temperature drops to ~34.8 °C, ~32.6 °C and ~33.4 °C with the cover of polymer film without and with artificial photonic structures ($D = 1$ and 4 µm, respectively). Obviously, the structural films with microspheres diameters of 1 µm and 4 µm can achieve larger temperature drop of ~ 2.2 °C and ~1.4 °C compared to that of the flat film, respectively. Considering the comparable thermal conductivity of the three samples,

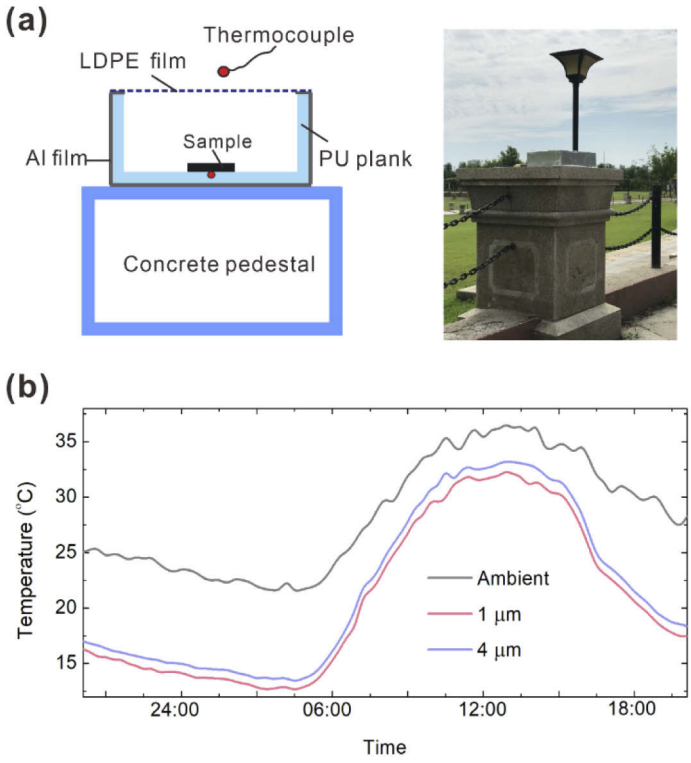

Fig. 3. (a) The illustration of the experimental set-up and the self-made device. (d) 24 h temperature measurement of the ambient and the radiation film (03/08/2020 20:00 to 04/08/2020 20:00).

Optics EXPRESS

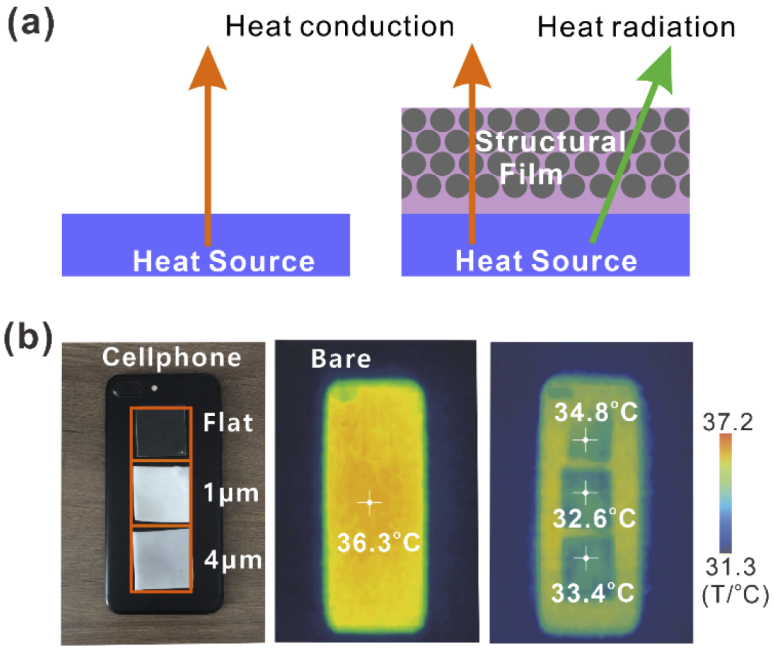

Fig. 4. (a) Schematic illustration of the heat dissipation without and with structural polymer film. (b) The infrared images of a cellphone rear cover after the removal of the radiator films. The corresponding infrared image of the bare rear cover is recorded for reference purposes.

the higher temperature drop can be attributed to more undesirable heat that can be radiated by the opal-like structured films from the hot surface. This feature implies that the structural polymer film could be potentially adopted for electronic devices package materials for better heat dissipation and desirable cooling efficiency.

3. Experimental section

Composited films Fabrication: Emulsifier-free emulsion polymerization method is employed to synthesize water-soluble, monodispersed PS microspheres [34,35]. To fabricate flexible composite film with artificial opal photonic crystals, the PS microsphere solution is dispersed on the silicon substrate and then thermally cured (70 °C, 2 h) to form opal-like photonic crystals template. Subsequently, the precursors of PDMS solution (premixed with 1/10 cross-linker, Dow Corning Co.) are spin-coated onto the surface of the as-prepared PS templates (4000 rpm for 50 s). Thereafter, the samples are put into a vacuum oven for annealing treatment (60 °C, 2 h). During the annealing processing, the precursors of PDMS solution is filtrated into the voids (~30 vol%) of the opal-like photonic crystals, and the structured films with built-in PS microspheres are obtained by peeling off the composite films from the silicon substrate. The thickness of the composite film is characterized as ~280 μm. To attain more evidence of the influence of artificial opal-like photonic crystals on radiative cooling, the flat PDMS films are also fabricated following the same fabrication conditions as presented above.

Optical Simulation: The finite-difference time-domain (FDTD) method is adopted to calculate the near-field distributions and absorptivity/emissivity spectra. The optical constants of the PDMS are determined according to the experimental measurement and the real and imaginary parts of the refractive index of PS are extracted from the previous literature [36]. In the simulation, the artificial opal-like PS microspheres are arranged as the FCC crystals structure, where a plane wave light source is incident along z axis. Perfect matched boundary (PML) boundary conditions

Optics EXPRESS

and periodic boundary conditions are adopted in z direction, and x, y directions, respectively. The absorption value is calculated according the equation of A = 1-R-T.

Characterization: The SEM images are attained using SEM (FEM, Quanta 250FEG). The total reflectivity spectra within the sunlight irradiation spectrum are measured by Lambda 950 (PerkinElmer) with an integrating sphere, and the reflection (R) and transmission (T) spectra in mid-infrared range are measured by a Fourier transform infrared spectrometer (FTIR, IRAffinity, Shimadzu) with an infrared integrating sphere. The IR digital images are recorded by a portable thermal imaging camera (T650sc, FLIR systems). The direct and diffuse solar irradiance is tested by an optical power meter (NEWPORT 1918-R). The Yong's modulus of the films is characterized by using material testing machine (Instron 5967). The film thickness is characterized using a probe profilometer (Veeco, Dektak 8).

4. Theory analysis

4.1. Cooling performance calculation

To numerically perform the cooling performance analysis for the as-prepared structural polymer films such as the net cooling power and temperature decrease, the energy balance state of the both daytime and nighttime passive radiative cooling are systematically investigated. Taking into all the heat exchange progress, the net cooling power of a radiator during daytime ($P_{net-day}$) and nighttime ($P_{net-night}$) can be respectively expressed as [37–39]:

$$P_{net-day}(T_{sample}) = P_{rad}(T_{sample}) - P_{atm} - P_{sun} - P_{cond+conv} \tag{1}$$

$$P_{net-night}(T_{sample}) = P_{rad}(T_{sample}) - P_{atm} - P_{cond+conv} \tag{2}$$

where T_{sample} is the temperature of the radiator, and the outward radiation power P_{rad} of the radiator is calculated by

$$P_{rad}(T_{sample}) = \int d\Omega cos\theta \int_0^\infty d\lambda I_{BB}(T_{sample}, \lambda)\varepsilon(\lambda, \theta) \tag{3}$$

where θ, λ and $\int d\Omega = 2\pi \int_0^{\frac{\pi}{2}} d\theta sin\theta$ represent the polar angle, the wavelength, and angular integral over a hemisphere, respectively. $\varepsilon(\lambda, \theta)$ represents the directional emissivity of the radiator at the wavelength of λ, which equals to its absorptivity according to Kirchhoff's law. The spectral radiance density $I_{BB}(T_{sample}, \lambda)$ of a blackbody at T_{sample} is

$$I_{BB}(T_{sample}, \lambda) = 2hc^2/\lambda^5 \left(e^{\frac{hc}{\lambda k T_{sample}}} - 1 \right) \tag{4}$$

here, h, c, k and λ represent the Planck's constant, the speed of light, the Boltzmann constant, and the wavelength, respectively. The absorbed thermal power P_{atm} due to incident atmospheric thermal radiation is given by

$$P_{atm}(T_{amb}) = \int d\Omega cos\theta \int_0^\infty d\lambda I_{BB}(T_{amb}, \lambda)\varepsilon(\lambda, \theta)\varepsilon_{atm}(\lambda, \theta) \tag{5}$$

where $\varepsilon_{atm}(\lambda, \theta) = 1 - t(\lambda)^{1/cos\theta}$ is the atmosphere's emissivity, T_{atm} is the ambient temperature, and $t(\lambda)$ is the atmospheric transmittance in the zenith direction. The incident solar irradiation power P_{sun} absorbed by the radiator is given as

$$P_{sun}(T_{sample}) = \int_0^\infty d\lambda \varepsilon(\lambda, \theta_{sun}) I_{AM1.5}(\lambda) \tag{6}$$

here, the $I_{AM1.5}(\lambda)$ denotes the solar illumination. The term $P_{cond+conv}$ is related to conduction and convection and is given by

$$P_{cond+conv} = h_c(T_{amb} - T_{sample}) \tag{7}$$

where h_c is heat transfer coefficient stemming from the conductive and convective heat exchange of the radiator with the surrounding ambient air.

Optics EXPRESS

The theoretical net cooling power and temperature decrease of structural films with built-in PS spheres (D =1 μm and 4 μm) are calculated via the equations (1) - (7) based on the measured data from reflection and transmission spectra and demonstrated in Figure 5 and Figure 6, respectively. As can be seen from Fig. 5, the temperature decreases with the increasing heat transfer coefficient h_c values because that the non-radiative heat contributes to power input when T_a exceeding T_s. More importantly, even with a heat transfer coefficient h_c = 6 W·m^{-2}·K^{-1}, the temperature reduction values of ~11 °C and ~26 °C can be still realized during daytime and nighttime for the microsphere-structured film (D = 1 μm), respectively. The temperature reduction difference between the daytime and nighttime demonstrates the importance of the high solar reflection to daytime radiative cooling. Notably, although the total reflectance and the average emissivity values of the structured film with microsphere diameters of 4 μm is slightly lower than that of the film with microsphere diameters of 1 μm, the corresponding theoretical net cooling power can still achieve ~112 W·m^{-2} and ~198 W·m^{-2} during daytime and nighttime, respectively (Fig. 6). Meanwhile, when h_c = 6 W·m^{-2}·K^{-1}, the temperature reduction of the film can approaches ~9 °C and ~24 °C during daytime and nighttime, respectively, also displaying favorable all-daytime passive radiative cooling performance compared with that of the polymer film with microsphere diameters of 1 μm. These results directly verify the important role of the built-in artificial opal-like crystal structures. It should be emphasized that there obviously exists the discrepancy between the theoretical calculation and the experimental results discussed above, which can be attributed to the evitable fluctuations of the temperature of the ambient stemming from some uncertain factors (*e.g.*, the sudden gust of wind).

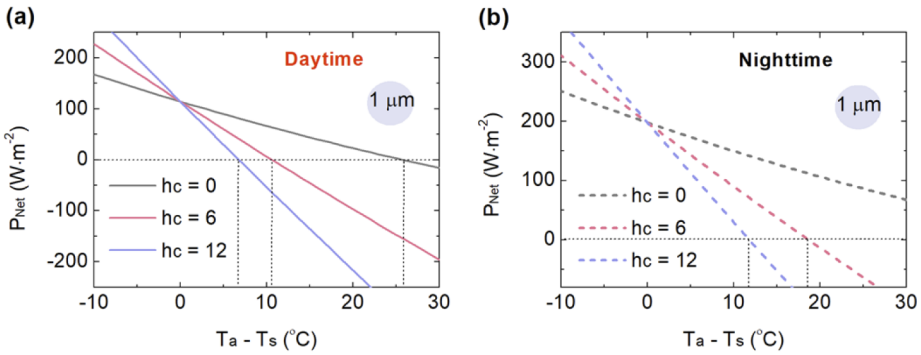

Fig. 5. Theoretical cooling power of the structural radiator film (D = 1 μm) as a function of temperature difference ($T_a - T_s$) with hc = 0, 6, 12 W·^{2}·K^{-1} during (a) daytime, and (b) nighttime. The T_a and T_s depict the temperature of the ambient air and the radiator surface and T_a is equals to 300 K.

4.2. Theoretical analysis

To further understand the physical mechanism of high MIR absorptivity in our proposed composite film, the calculated emissivity and electric field distributions are carefully investigated. Figure 7(a) presents the real and imaginary parts of the complex index of PS and PDMS materials within the wavelength regime of 0.3 ~ 20 μm. It can be directly deduced that sunlight absorption can be negligible for both materials because that the imaginary parts of both materials are close to zero within the whole solar spectrum (0.3 ~ 2.5 μm). This is one of the key features for realizing diurnal passive radiative cooling [32,40]. Moreover, the high values of imaginary parts of PDMS material beyond 8 μm correspond to high absorptivity bands [41]. This high absorption/emission region coincides with the Earth's atmosphere window, enabling thermal radiative transfer from PDMS material to the thermal reservoir of the outer space. In addition, the real parts difference

Optics EXPRESS

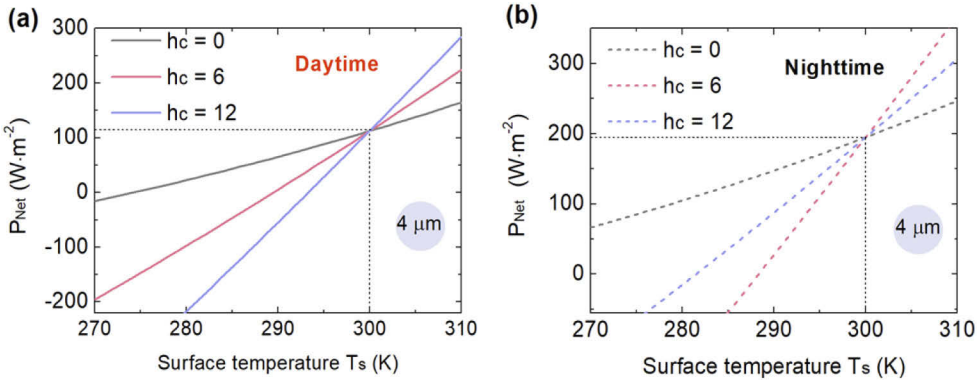

Fig. 6. Theoretical cooling power of the structural radiator film ($D = 4\,\mu m$) as a sample surface temperature T_s . with hc = 0, 6, 12 $W{\cdot}m^{-2}{\cdot}K^{-1}$ during (a) daytime, and (b) nighttime.

between the of PS microsphere arrays and PDMS material in the whole solar spectra enabling forming opal-like crystal structures [42], resulting in the favorable sunlight reflection as discussed in Fig. 2(a).

To reveal the emissivity capability of the films within the MIR range, the emissivity spectra of the PDMS films with and without artificial opal-like crystal structures are calculated and displayed in Fig.7b. It can be observed that the emissivity of the structural films decreases as the diameter of the PS sphere increases monotonically, and that emissivity of the microsphere-structured film with diameter of 5 μm is comparable to that of the bare film while a favorably higher emissivity is acquired when the diameter is around 1 μm. This feature may stem from weaker local resonances triggered when the increasing diameter of the PS microsphere approaches close to the wavelength of the impinging MIR wave light. Therefore, to clearly clarify our designed film structure, we chose PS particles with sizes of 1 μm and 4 μm for our previously conducted experiments. This result corresponds well with the experimentally measured absorptivity in Fig. 2(e) considering that the reasonable and evitable experimental errors originating from fabrication and measurement procedures.

To gain a deep insight into the light trapping mechanisms within MIR range of artificial opal-like crystal structures built-in composite films, we performed optical modeling simulations using the finite difference time domain (FDTD) method (see the details in the Experimental section). Fig. 8 illustrates the normalized electric near-field distributions of the film without and with opal-like structures. Compared with the slow and uniform absorption of the flat film (Figure 8(a)), the embedded opal-like structure plays a crucial role in the high absorptivity/emissivity within MIR region at three representative wavelengths (Fig. 8(b-c)). The built-in PS microsphere arrays forming three-dimensional opal-like structures, which can support the electric near-field resonant in a wide band of spectrum and further enhanced and broaden the absorptivity band. Moreover, the electric near-field resonant is not just localized within the microspheres, but diffuses into the adjacent layers which can support the optical resonance modes together. Overall, the high absorptivity of the composite film in the atmospheric windows can be ascribed to both the high extinction capability of PDMS material and the strong broadband electric near-filed resonance induced by the introduced artificial opal structures. It should be noted that although the measured emissivity trend of the films is consistent with the electric near-field distributions, the enhanced emissivity of the structured films is not as high as that they seemingly should be. The difference between the experiment and the theory can be attributed to inevitable defects within the artificial

Optics EXPRESS

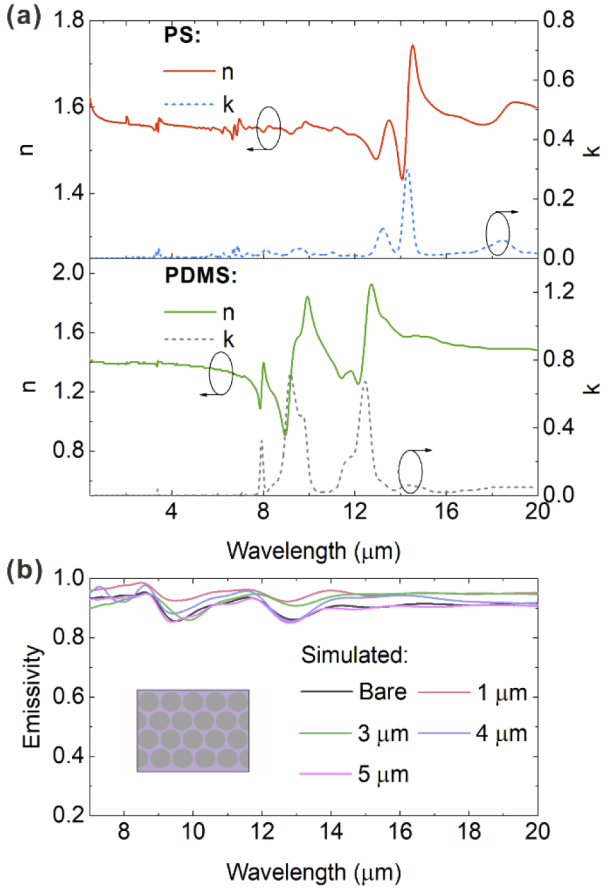

Fig. 7. (a) The real and imaginary parts of the complex index of PS and PDMS within the wavelength regime of 0.3 ~ 20 μm. (b) The calculated emissivity of the films within the MIR range without and with artificial opal-like crystal structures. Inset depicts the schematic cross-section opal-like crystal structure. The thickness of the film is set as 280 μm.

opal structures induced by the fabrication procedures and long range quasi-periodic distribution of the PS microsphere arrays.

Optics EXPRESS

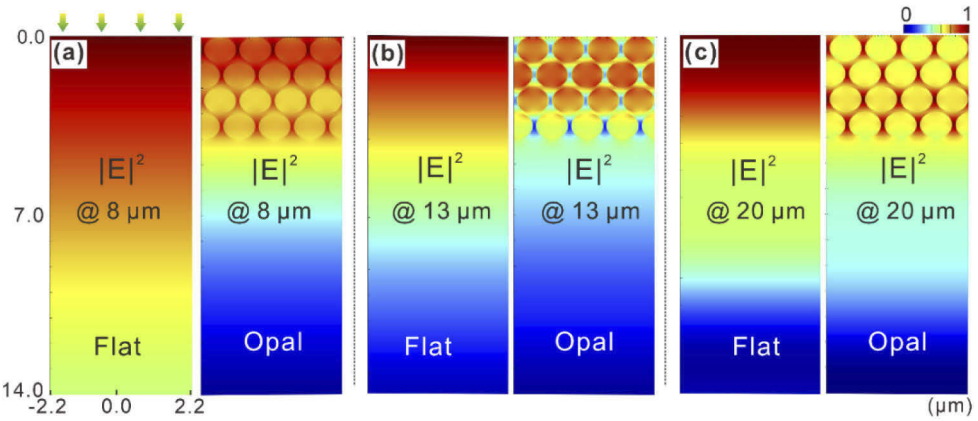

Fig. 8. Simulated electric field profiles of the flat and structured films at (a) 8 μm, (b) 13 μm and (c) 20 μm, respectively.

5. Conclusion

In summary, we have demonstrated and fabricated a flexible composite film with built-in artificial opal structures for highly efficient day- and nighttime passive radiative cooling. This structural composite film exhibits sufficiently high solar reflectance of ~92.7% in the major sunlight region and a thermal emittance of ~93.6% within the atmospheric window. The introduced opal-like structures embedded in PDMS film plays a crucial role for scattering the impinging sunlight and inducing the light trapping within the MIR region simultaneously. Without needing any traditional reflector encompassing silver or aluminum foils, the optimal composite film realizes subambient temperature reduction of ~4.8 °C under direct sunshine and ~8.5 °C during the night. The presented approach provides an alternative way to design and fabricate efficient all-day passive radiative cooling materials for various promising applications such as radiative cooling textile, cold-chain transportation and energy-efficient building.

Funding. National Natural Science Foundation of China (61775076), Qinglan Project of Jiangsu Province of China; Natural Science Research of Jiangsu Higher Education Institutions of China (20KJB140021); Natural Science Foundation of Jiangsu Province (BK20201067); Natural Science Foundation of Jiangsu Province (BK20201476).

Disclosures. The authors declare no conflicts of interest.

Data availability. Data underlying the results presented in this paper are not publicly available at this time but may be obtained from the authors upon reasonable request.

References

1. J. Mandal, Y. Fu, A. C. Overvig, M. Jia, K. Sun, N. N. Shi, H. Zhou, X. H. Xiao, N. Yu, and Y. Yang, "Hierarchically porous polymer coatings for highly efficient passive daytime radiative cooling," Science **362**(6412), 315–319 (2018).
2. L. Li, Y. Li, H. Yu, and Y. L. He, "A feedforward-feedback hybrid control strategy towards ordered utilization of concentrating solar energy," Renewable Energy **154**, 305–315 (2020).
3. D. Li, X. Liu, W. Li, Z. Lin, B. Zhu, Z. Li, J. Li, B. Li, S. Fan, J. Xie, and J. Zhu, "Scalable and hierarchically designed polymer film as a selective thermal emitter for high-performance all-day radiative cooling," Nat. Nanotechnol. **16**(2), 153–158 (2021).
4. E. Rephaeli, A. Raman, and S. Fan, "Ultrabroadband photonic structures to achieve high-performance daytime radiative cooling," Nano Lett. **13**(4), 1457–1461 (2013).
5. M. M. Hossain and M. Gu, "Radiative cooling: principles, progress, and potentials," Adv. Sci. **3**(7), 1500360 (2016).
6. B. Zhao, M. Hu, X. Ao, N. Chen, Q. Xuan, D. Jiao, and G. Pei, "Performance analysis of a hybrid system combining photovoltaic and nighttime radiative cooling," Appl. Energy **252**, 113432 (2019).
7. A. R. Gentle and G. B. Smith, "Radiative heat pumping from the earth using surface phonon resonant nanoparticles," Nano Lett. **10**(2), 373–379 (2010).
8. Y. Zhai, Y. Ma, S. N. David, D. Zhao, R. Lou, G. Tan, R. Yang, and X. Yin, "Scalable-manufactured randomized glass-polymer hybrid metamaterial for daytime radiative cooling," Science **355**(6329), 1062–1066 (2017).

Optics EXPRESS

9. S. Meng, L. Long, Z. Wu, N. Denisuk, Y. Yang, L. Wang, F. Cao, and Y. Zhu, "Scalable dual-layer film with broadband infrared emission for sub-ambient daytime radiative cooling," Sol. Energy Mater. Sol. Cells **208**, 110393 (2020).
10. B. Xiang, X. Yin, and J. Zhang, "A novel cool material: ASA (acrylonitrile-styrene-acrylate) matrix composites with solar reflective inorganic particles," Compos. Sci. Technol. **145**, 149–156 (2017).
11. Z. Yang, T. Jiang, and J. Zhang, "Passive daytime radiative cooling inorganic-polymeric composite artificial lawn for the alternative to the natural lawn," Sol. Energy Mater. Sol. Cells **219**, 110783 (2021).
12. J. Song, J. Qin, J. Qu, Z. Song, W. Zhang, X. Xue, Y. Shi, T. Zhang, W. Ji, and R. Zhang, "The effects of particle size distribution on the optical properties of titanium dioxide rutile pigments and their applications in cool non-white coatings," Sol. Energy Mater. Sol. Cells **130**, 42–50 (2014).
13. A. P. Raman, M. Abou Anoma, L. Zhu, E. Rephaeli, and S. Fan, "Passive radiative cooling below ambient air temperature under direct sunlight," Nature **515**(7528), 540–544 (2014).
14. K. Zhou, W. Li, B. B. Patel, R. Tao, Y. Chang, S. Fan, Y. Diao, and L. Cai, "Three-dimensional printable nanoporous polymer matrix composites for daytime radiative cooling," Nano Lett. **21**(3), 1493–1499 (2021).
15. Z. Yang, H. Sun, Y. Xi, Y. Qi, Z. Mao, P. Wang, and J. Zhang, "Bio-inspired structure using random, three-dimensional pores in the polymeric matrix for daytime radiative cooling," Sol. Energy Mater. Sol. Cells **227**, 111101 (2021).
16. L. Zhou, J. T. Zhao, H. Y. Huang, F. Nan, G. H. Zhou, and Q. D. Ou, "Flexible polymer photonic films with embedded microvoids for high-performance passive daytime radiative cooling," ACS Photonics **8**(11), 3301–3307 (2021).
17. T. Li, Y. Zhai, S. He, W. Gan, Z. Wei, M. Heidarinejad, D. Dalgo, R. Mi, X. Zhao, J. Song, J. Dai, C. Chen, A. Alili, A. Vellore, A. Martini, R. Yang, J. Srebric, X. Yin, and L. Hu, "A radiative cooling structural material," Science **364**(6442), 760–763 (2019).
18. J. Mandal, M. Jia, A. Overvig, Y. Fu, E. Che, N. Yu, and Y. Yang, "Porous polymers with switchable optical transmittance for optical and thermal regulation," Joule **3**(12), 3088–3099 (2019).
19. X. Wang, X. Liu, Z. Li, H. Zhang, Z. Yang, H. Zhou, and T. Fan, "Scalable flexible hybrid membranes with photonic structures for daytime radiative cooling," Adv. Funct. Mater. **30**(5), 1907562 (2020).
20. W. Gao, Z. Lei, K. Wu, and Y. Chen, "Reconfigurable and renewable nano-micro-structured plastics for radiative cooling," Adv. Funct. Mater. **31**(21), 2100535 (2021).
21. I. M. Urrutia-Ortega, L. G. Garduño-Balderas, N. L. Delgado-Buenrostro, V. Freyre-Fonseca, J. O. Flores-Flores, A. González-Robles, J. Pedraza-Chaverri, and Y. I. Chirino, "Food-grade titanium dioxide exposure exacerbates tumor formation in colitis associated cancer model," Food Chem. Toxicol. **93**, 20–31 (2016).
22. C. I. Aguirre, E. Reguera, and A. Stein, "Tunable colors in opals and inverse opal photonic crystals," Adv. Funct. Mater. **20**(16), 2565–2578 (2010).
23. S. Y. Lee, S. H. Kim, H. Hwang, J. Y. Sim, and S. M. Yang, "Controlled pixelation of inverse opaline structures Towards reflection-mode displays," Adv. Mater. **26**(15), 2391–2397 (2014).
24. J. Liu, Z. Zhou, J. Zhang, W. Feng, and J. Zuo, "Advances and challenges in commercializing radiative cooling," Mater. Today Phys. **11**, 100161 (2019).
25. S. G. Kim, Y. G. Seo, Y. J. Cho, J. S. Shin, S. C. Gil, and W. M. Lee, "Optimization of emulsion polymerization for submicron-sized polymer colloids towards tunable synthetic opals," Bull. Korean Chem. Soc. **31**(7), 1891–1896 (2010).
26. H. Fudouzi, "Fabricating high-quality opal films with uniform structure over a large area," J. Colloid Interface Sci. **275**(1), 277–283 (2004).
27. L. J. Guo, "Nanoimprint lithography: methods and material requirements," Adv. Mater. **19**(4), 495–513 (2007).
28. C. Lopez, "Materials aspects of photonic crystals," Adv. Mater. **15**(20), 1679–1704 (2003).
29. S. H. Kim, S. J. Jeon, W. C. Jeong, H. S. Park, and S. M. Yang, "Optofluidic synthesis of electroresponsive photonic janus balls with isotropic structural colors," Adv. Mater. **20**(21), 4129–4134 (2008).
30. J. Zhang, Z. Zhou, J. Quan, D. Zhang, J. Sui, J. Yu, and J. Liu, "A flexible film to block solar radiation for daytime radiative cooling," Sol. Energy Mater. Sol. Cells **225**, 111029 (2021).
31. U. Banik, K. Sasaki, N. Reininghaus, K. Gehrke, M. Vehse, M. Sznajder, T. Sproewitz, and C. Agert, "Enhancing passive radiative cooling properties of flexible CIGS solar cells for space applications using single layer silicon oxycarbonitride films," Sol. Energy Mater. Sol. Cells **209**, 110456 (2020).
32. X. Yin, R. Yang, G. Tan, and S. Fan, "Terrestrial radiative cooling: Using the cold universe as a renewable and sustainable energy source," Science **370**(6518), 786–791 (2020).
33. A. Srinivasan, B. Czapla, J. Mayo, and A. Narayanaswamy, "Infrared dielectric function of polydimethylsiloxane and selective emission behavior," Appl. Phys. Lett. **109**(6), 061905 (2016).
34. X. Du and J. He, "Facile size-controllable syntheses of highly monodisperse polystyrene nano-and microspheres by polyvinylpyrrolidone-mediated emulsifier-free emulsion polymerization," J. Appl. Polym. Sci. **108**(3), 1755–1760 (2008).
35. B. Yang, L. Xu, Y. Liu, B. Liu, and M. Zhang, "Preparation of monodisperse polystyrene microspheres with different functional groups using soap-free emulsion polymerization," Colloid Polym. Sci. **299**(7), 1095–1102 (2021).
36. X. Zhang, J. Qiu, X. Li, J. Zhao, and L. Liu, "Complex refractive indices measurements of polymers in visible and near-infrared bands," Appl. Opt. **59**(8), 2337–2344 (2020).
37. Z. Wang, D. Kortge, J. Zhu, Z. Zhou, H. Torsina, C. Lee, and P. Bermel, "Lightweight, passive radiative cooling to enhance concentrating photovoltaics," Joule **4**(12), 2702–2717 (2020).

Optics EXPRESS

38. B. Zhao, M. Hu, X. Ao, N. Chen, Q. Xuan, Y. Su, and G. Pei, "A novel strategy for a building-integrated diurnal photovoltaic and all-day radiative cooling system," Energy **183**, 892–900 (2019).
39. B. Xiang, R. Zhang, Y. Luo, S. Zhang, L. Xu, H. Min, S. Tang, and X. Meng, "3D porous polymer film with designed pore architecture and auto-deposited SiO_2 for highly efficient passive radiative cooling," Nano Energy **81**, 105600 (2021).
40. L. Zhou, H. Song, J. Liang, M. Singer, M. Zhou, E. Stegenburgs, N. Zhang, C. Xu, T. Ng, Z. Yu, B. Ooi, and Q. Gan, "A polydimethylsiloxane-coated metal structure for all-day radiative cooling," Nat. Sustain. **2**(8), 718–724 (2019).
41. D. Cai, A. Neyer, R. Kuckuk, and H. M. Heise, "Raman, mid-infrared, near-infrared and ultraviolet-visible spectroscopy of PDMS silicone rubber for characterization of polymer optical waveguide materials," J. Mol. Struct. **976**(1-3), 274–281 (2010).
42. H. H. Kim, E. Im, and S. Lee, "Colloidal photonic assemblies for colorful radiative cooling," Langmuir **36**(23), 6589–6596 (2020).